Contrast Enhancement of Electron Magnetic Resonance Images Using Linear and Nonlinear Unsharp Masking Techniques

P. Alli
Avinashilingam Deemed University,
Coimbatore-641108
alli_rajus@yahoo.com

Murali C Krishna
National Cancer Institute,
Bethesda, Maryland 20892
murali@helix.nih.gov

R. Murugesan
Madurai Kamraj University,
Madurai-625021
rammku@eth.net

Abstract

This paper presents an evaluation of various unsharp masking techniques for enhancement of Electron Magnetic Resonance (EMR) images. Both the linear and non-linear unsharp masking techniques are tested for contrast enhancement of continuous wave EMR images. In vivo EMR renal images as well as leg-tumor images of a mouse are used as test images. Both visual appearance as well as Signal to Noise Ratio (SNR) are used as the metrics of evaluation. The results suggest that adaptive unsharp masking technique performs well for EMR image enhancement, compared to the other approaches.

1. Introduction

Electron Magnetic Resonance Imaging (EMRI) is an emerging biomedical imaging technology for direct detection, characterization and quantification of free radicals in chemical and biological systems [4, 11]. The sensitivity of EMR spectral properties (hyperfine splitting, line width) to physiological parameters such as pH, pO2 and viscosity makes EMRI a potentially powerful functional imaging technique [9]. EMRI is akin to MRI, but endogenous paramagnetic imaging agents are to be administered for the acquisition of *in vivo* EMR images. The imaging agents should be used in lower concentration to avoid toxicity. This low dose leads to weak EMR images. In addition, the EMR imager also operates at lower frequencies to obtain sufficient tissue penetration. The low frequency operation also results in loss of sensitivity, leading to poor image quality. Hence to develop EMR imaging modality as a viable biomedical tool, novel image analysis methods need to be developed and evaluated.

Generally, in biomedical imaging, the resolution of individual anatomical structures is of prime importance for diagnostic purposes and treatment planning [6]. Feature detection and image resolution can be improved by sharpening some features by decreasing the ambiguity between different regions of the image. There have been several approaches to enhance Magnetic Resonance Images (MRI) without edge degradation [3, 2]. These methods are used to improve the visual appearance of MR images. So far no attempt has been made to evaluate filters for the enhancement of EMR images. Hence in this paper, both linear and nonlinear filters are investigated based on the unsharp masking technique. A comparative evaluation is presented based on both visual appearance as well SNR of the output images.

2. EMR Image Acquisition

Radio Frequency (RF) EMR imaging uses both Fourier Transform (FT) and Continuous Wave(CW)techniques [9, 1, 8]. The images used in the present study were acquired using a RF CW EMR imager. The EMR imager operates at a nominal frequency of 300 MHz corresponding to a resonant magnetic field of 106 G (10.6 mT) for g = 2 spin systems. A detailed description of the 300 MHz imager along with the sensitivity and imaging protocols are furnished elsewhere [5].

A home-built parallel coil resonator (25 mm x 25 mm) was used for imaging. Two derivatives of symmetric trityl based free radicals, abbreviated as Oxo63 and Oxo31 were used as imaging agents [9]. Animal imaging was performed following the guide for the care and use of laboratory animals prepared by the institute of laboratory animal resources, National Research Council. A mixture of ketamine (90 mg/kg of body weight) and xylazine (30 mg/kg of body weight) was used to anesthetize (i.p. or i.v.) a C3H mouse that was placed (lying on its back) in the parallel coil resonator. After intravenous injection of the imaging agent (100-200 μL) of a 20 mM Oxo63 in Phosphate Buffer Solution (PBS), the image data acquisition was initiated. For the evaluation of the different filters, three sets of *invivo* murine EMR images were taken. One set consisting a sequence of temporal images was taken to depict the renal clearance of the imaging agent. The second one used is a high resolution kidney image. The third one showing a tumor induced in the leg of a mouse was also used to test the system.

3. Theory

3.1. Linear Unsharp Masking (LUM)

Classic linear unsharp masking scheme shown in Figure 1, is often used to enhance the visual appearance of an image. In this technique, a high pass filtered and and

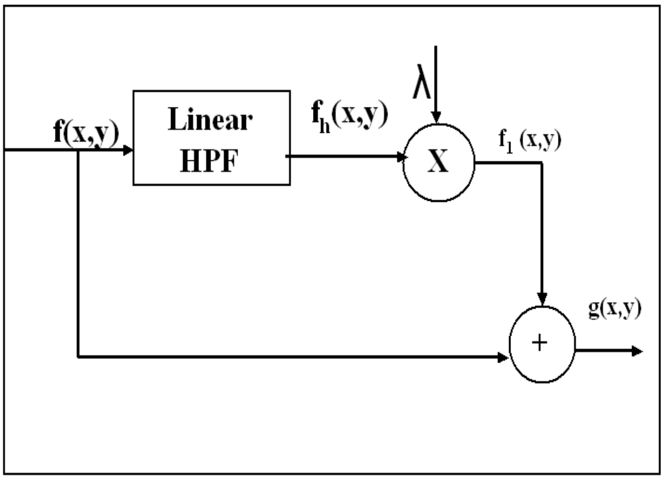

Figure 1: Linear unsharp masking

scaled version of the input image is added with the input image, to obtain the result [7]. This filter has good sharpening effect but is very sensitive to noise and leads to undesirable distortions.

3.2. Order Statistics Laplacian Filter (OSLF)

Different approaches have been made to address the noise sensitivity of the LUM scheme. These approaches are based on the use of nonlinear operators in the correction path. One such attempt uses order statistics Laplacian filter to overcome the limitations of LUM. Laplacian filter is an edge enhancing and sharpening filter which can be implemented by $F - \nabla^2 F$, where F is an image, and $\nabla^2 F$ is the Laplacian operator, given by

$$\nabla^2 F(i,j) = L[A(i,j) - F(i,j)] \qquad (1)$$

Here L is the number of samples inside window centered at (i,j), A(i,j) is the average of the samples inside the window and F(i,j) is the current pixel of the original image. However, the Laplacian operator is also sensitive to noise. To reduce the noise sensitivity, the Laplacian is often used after some prefiltering. The order statistics Laplacian operator reduces the noise amplification when the input disturbance is a zero mean and a white Gaussian process. This OSLF operator, $OS\nabla^2 F$, is given by

$$\nabla^2 F(i,j) = L[A(i,j) - M(i,j)] \qquad (2)$$

Here M(i,j) is the sample median of values inside the window. The OS Laplacian is equal to the digital Laplacian whenever the center value of the window F(i,j) equals the median M(i,j) [10]. Even though OSLF is not as sensitive to noise as LUM, its edge enhancing characteristic is not very significant.

3.3. Adaptive Unsharp Masking Technique (AUM)

Linear filtering techniques often reduce the amplitude of noise fluctuations, but also degrade the sharp details such as edges and lines. In medical image processing, preservation of small structures and region boundaries are very important. Image degradation and information loss are not acceptable. Adaptive filtering techniques satisfy the requirements of medical image processing. One such adaptive technique that overcomes the problem of OSLF is adaptive unsharp masking (AUM) filtering scheme shown in Figure 2. AUM mod-

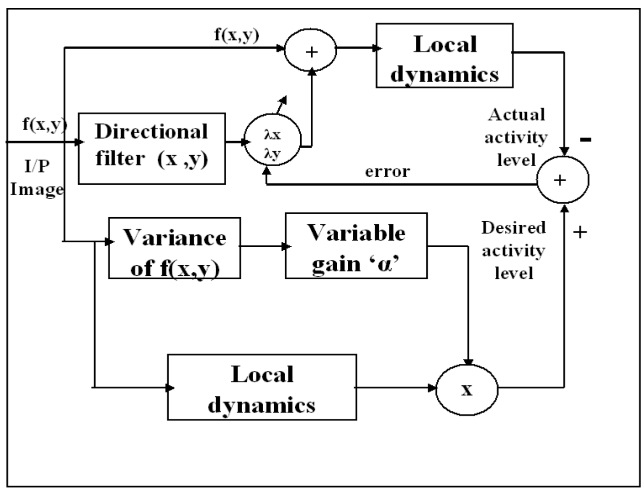

Figure 2: Adaptive unsharp masking

ifies the medium contrast details in the input image more than the large contrast details to avoid overshoot in the output image [7]. For implementation of AUM, in the present work, the desired activity level and the actual activity level were calculated and the difference between them was made as minimum as possible. The desired activity level of the image was estimated by measuring the local variance of the image. The computation of the local variance of the given image was made over a 3x3 pixel block, using the equation,

$$v_i(n,m) = \frac{1}{2}\sum_{i=(n-1)}^{n+1}\sum_{j=m-1}^{m+1}(x(i,j) - \overline{x}(n,m))^2 \quad (3)$$

Here $\overline{x}(n,m)$ is the average grey level and $x(i,j)$ is the instantaneous grey level value. The classification of the input image as belonging to smooth, medium contrast and high contrast regions was done based on the computed local variance ranges. In the present study, the classification was carried out based on the positive thresholds denoted as τ_1 and τ_2. For all the three EMR images, optimal values for τ_1 and τ_2 were found to be 70 and 190 respectively after testing with values ranging from 0 to 250. The input signal was classified as a smooth region if $v_i(n,m) < \tau_1$, a medium contrast area if $\tau_1 \leq v_i(n,m) < \tau_2$ and a high contrast area otherwise [7]. The variable gain 'α' was selected based on the above three levels. For EMR images, for the smooth region, the gain was taken as unity, for medium contrast area it was chosen as greater than 1 and for high contrast area it was taken between the above two values of 'α' (unity and greater than unity). The local dynamics of the input image was calculated by the corresponding 3 X 3 mask. The computed result was multiplied with the already calculated variable gain 'α' to get the desired activity level $g_d(n,m)$, where,

$$g_d(n,m) = \alpha(n,m)g_x(n,m) \quad (4)$$

The actual activity level of the image was computed by finding the local dynamics of the sum of the filtered output and original image [7]. The filtered outputs were controlled by the scaling factors $\lambda_x(n,m)$ and $\lambda_y(n,m)$ independently and are expressed by the equation

$$y(n,m) = x() + \lambda_x() * z_x() + \lambda_y()z_y() \quad (5)$$

The controlled filtered outputs were added back to the input image x(n,m). The cost function based on the error which is the difference between the actual activity level and the desired activity level was computed using the equation,

$$J(n,m) = E[e^2(n,m)] = E[(g_d(n,m) - g_y(n,m))^2] \quad (6)$$

The adaptive algorithm was implemented recursively to change the scaling vector such that $J(n,m)$ was as small as possible for the whole image. Gauss- Newton algorithm was used to compute the scaling vector using

$$\Lambda(n,m+1) = \Lambda(n,m) - \mu R^{-1}(n,m) \cdot \partial \frac{\partial}{\partial \Lambda(n,m)} \quad (7)$$

$$(e^2(n,m)) = \Lambda(n,m) + 2\mu e(n,m)R^{-1}(n,m)G^T(n,m) \quad (8)$$

Here $R(n,m)$ is an estimate of autocorrelation matrix of the input vector $G(n,m)$, and it was computed recursively by

$$R(n,m) = (1-\beta)R(n,m-1) + \beta G(n,m)G^T(n,m) \quad (9)$$

The convergence parameter, β, a small positive step size to control the speed of convergence of the adaptive filter, was chosen after trial and error as 0.4 or 0.5 for the EMR images.

4. System Implementation

The system was developed using C language for its computational speed and portability. For reading the input images and to view their corresponding output, a well designed graphical user interface was developed. For user friendliness, interactive facilities were included to feed the parameters. The required filter for implementation could be selected independently. The overall system was based on a modular architecture. All the modules were linked with the front-end menu for user friendliness. Resultant images (along with their SNR values) could be readily viewed with their input to facilitate comparison.

5. Results and Discussion

The various filters described in this paper were evaluated for their performance by selecting three sets of *in vivo* murine EMR Images. Figure 3(a) presents renal imaging of a mouse showing progressive redistribution of the imaging agent, predominantly in the two kidneys and the bladder.

Figure 4(a) shows a high resolution kidney image (three times higher resolution than Figure 3(a). Figure 5(a) shows EMR images of the legs of a mouse, with a tumor in the right hind leg of the animal. Visual evaluation was used in the first stage.

5.1. Visual Evaluation

5.1.1. Kidney and Bladder Images

Figure 3. presents the results of the enhancement of different filters. The EMR image taken at 2.8 min af-

ter the administration of the imaging agent is shown in Figure 3(a). The imaging agent localization in the two kidneys and the bladder is shown. But the distribution of the spin probe is not clear in the image. This is the input image to the three filters studied. Figure 3(b) shows the output of LUM. A very slight little enhancement is observable. The output of OSLF shown in Figure 3(c) shows considerable enhancement without background noise amplification. The uniform areas are not disturbed. However, there is no significant enhancement in high detailed area, where more edge information are present. The AUM filtered image (Figure 3(d)) shows an improved differentiation of adjacent regions of similar intensity characteristics. The intensity variations are clearly visible and the contours corresponding to the two kidneys and the bladder are also seen clearly with high intensity variation.

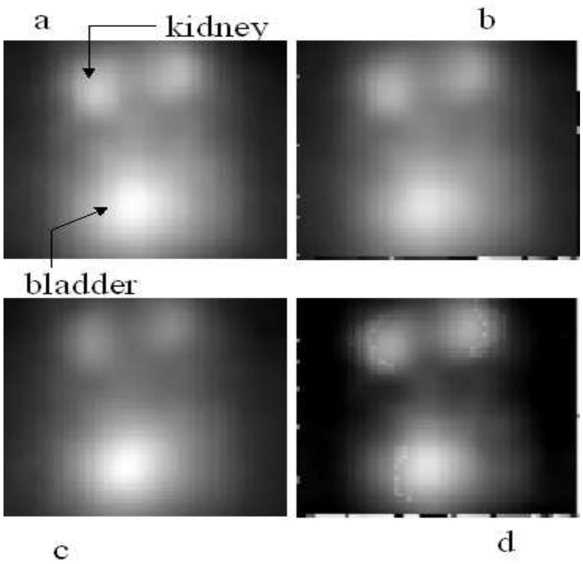

Figure 3: Evaluation the filters for enhancement of renal murine images. Output images of LUM (b), OSLF (c) and AUM (d) are shown along with the input image (a)

5.1.2. Kidney Images

Figure 4. shows the results of the experiments on applying the different algorithms to the high resolution kidney images. While LUM filter (Figure 4(b)) shows very little improvement, OSLF filter (Figure 4(c)) shows considerable enhancement in the image quality. Also the uniform areas not disturbed. But, the fine details are not visible in the high detailed area. The output of AUM, given in Figure 4(d), shows sufficient noise smoothing in flat regions and simultaneously good sharpening in the detailed areas. The contours of the organs are clearly delineated in the AUM filtered image in comparison to the other two filters.

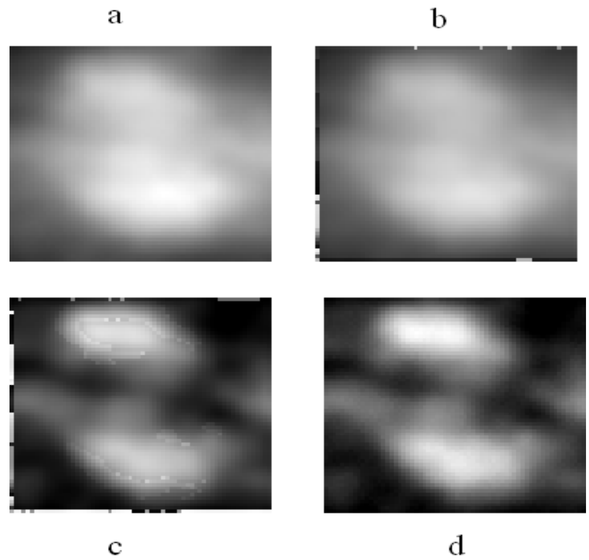

Figure 4: Enhancement of high resolution kidney EMR images. Output images of LUM (b), OSLF (c) and AUM (d) are shown along with the input image (a)

5.1.3. Murine Leg Tumor Images

Figure 5(a) shows 2D spatial EMR images of the imaging agent distribution in the normal and tumor bearing legs. Figure 5(b) shows the less enhanced image of the LUM filter. Only blurred edges are seen in this output. In Figure 5(c), the output of OSLF filter with comparatively higher enhancement is shown. However, the edges of the tumor are not clearly identified. The enhanced images of AUM filter shows the highest performance compared to the other filters. Thus the AUM technique performs consistently better for all the three EMR image data sets used for testing.

5.2. Calculation of Signal to Noise Ratio (SNR)

In addition to visual examination, the performance of the filters were examined more deeply by computing the SNR values. SNR is usually expressed in dB, in terms of peak values for impulse noise and root-mean-square values for random noise. In the present study, to compute SNR, first a 3 X 3 pixel kernel was constructed from the original image and its mean was calculated.

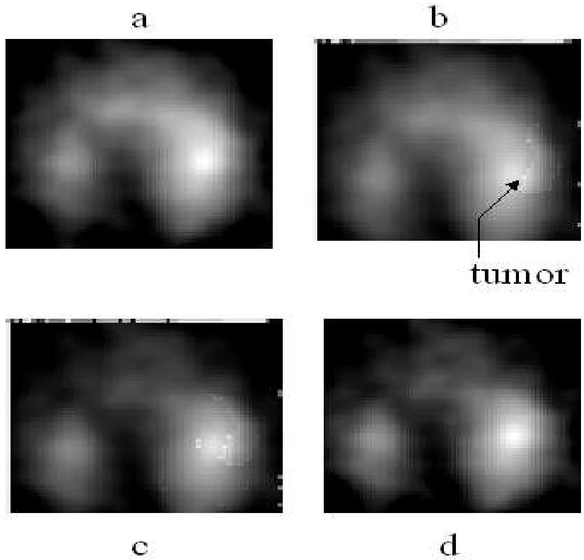

Figure 5: Enhancement of murine leg tumor EMR image. Output images of LUM (b), OSLF (c) and AUM (d) are shown along with the input image (a)

This mean value was subtracted from the central pixel of the kernel. Finally, the variance was computed using the expression,

$$Var(x,y) = \frac{1}{9}\sum^{n+1}\sum^{m+1}[F(i,j) - F'(x,y)]^2 \qquad (10)$$

Here F'(x,y) is the mean value and F(i,j) is the central pixel value.Table 1 gives the comparative SNR values (in dB) for all the three filters.

EMRI	INPUT	LUM	OSLF	AUM
Kidneybladder	2.06	2.12	2.14	3.01
Kidney	2.03	2.05	2.41	3.11
Mu.Leg tumour	2.01	2.21	2.31	3.01

Table 1: Quantitative estimate of performance evaluation as given by SNR (dB)

It is clearly seen from Table 1 that SNR value of adaptive unsharp masking technique is higher compared to the other filters.

6. Conclusion

Both linear and nonlinear unsharp masking techniques are evaluated for their potential as a viable tool for enhancement of EMR images. Both visual as well as quantitative SNR computation methods are used as metrics for evaluation. The adaptive unsharp masking technique shows good sharpening effects in detailed areas without degrading the homogeneous areas of the EMR images. It also enhances the medium contrast details better than other filter techniques investigated. Our study suggests the adaptive unsharp masking to be a suitable technique for EMR image enhancement.

References

[1] M. Afeworki, J.Cook, G. M. V. Dam, N. Devasahayam, D. Coffin, J. Larsen, J. Mitchell, R. Murugesan, S. Subramanian, and M. Krishna. Three dimensional whole body imaging of spin probes in mice by time-domain radio frequency electron paramagnetic resonance. *Magn. Reson*, (43), April 2000.

[2] C. Ann, Y. Song, and D. Park. Adaptive template filtering for signal to noise ratio enhancement in mri. *IEEE Transactions on Medical Imaging*, 18(6), June 1999.

[3] G. Gerig, O.Kubler, R.Kikinis, and F. A. Jolesz. Nonlinear anisotropic filtering of mri data. *IEEE Transactions on Medical Imaging*, 11(2), June 1992.

[4] L. Keselbrener, Y. Shimoni, and S. Akselrod. Nonlinear filters applied on computerized axial tomography: theory and phantom images. *Med phys*, 19(4), June 1992.

[5] J. Koscielniak, N. Devasahayam, M. Moni, P. Kuppusamy, K. Yamada, J. Mitchell, M. Krishna, and S. Subramanian. 300 mhz continuous wave epr spectrometer for small animal in vivo imaging. *Review of scientific instruments*, 71(11), April 2000.

[6] G. McGibney and M. Smith. An unbiased signal to noise ratio measure for magnetic resonance images. *Med. Phy.*, 20(4), July/August 1993.

[7] A. Polesel, G. Ramponi, and V. J. Mathews. Image enhancement via adaptive unsharp masking. *IEEE transactions on image processing*, 9(3), March 2000.

[8] S. Subramanian, K. Yamada, A. Irie, R. Murugesan, J. Cook, N. Devasahayam, G. V. Dam, J. Mitchell, and M. Krishna. Non-invasive in vivo oxymetric imaging by radio frequency ft epr. *Magnetic Resonance in Medicine*, (47), April 2002.

[9] K. Yamada, R.Murugesan, N. Devasahayam, J. Cook, J. Mitchell, S. Subramanian, and M. Krishna. Evaluation and comparison of pulsed and continuous wave radio frequency electron paramagnetic resonance techniques for in vivo detection and imaging of free radicals. *Journal of magnetic resonance*, (154), Nov 2002.

[10] Y.H.Lee and S.Y.Park. A study of convex/concave edges and edge enhancing operators based on the laplacian. *IEEE Trans. Circuits Syst*, (37), July 1990.

[11] A. Zavaljevski, A. Dhawan, M. Gaskil, W. Ball, and J. Johnson. Multi-level adaptive segmentation of multi-parameter mr brain images. *Computerized Medical Imaging and Graphics*, (24), Jan 2000.